

# A local approach to parameter space reduction for regression and classification tasks

Francesco Romor\*, Marco Tezzele† and Gianluigi Rozza‡

Mathematics Area, mathLab, SISSA, via Bonomea 265, I-34136 Trieste, Italy

July 26, 2021

## Abstract

Frequently, the parameter space, chosen for shape design or other applications that involve the definition of a surrogate model, present subdomains where the objective function of interest is highly regular or well behaved. So, it could be approximated more accurately if restricted to those subdomains and studied separately. The drawback of this approach is the possible scarcity of data in some applications, but in those, where a quantity of data, moderately abundant considering the parameter space dimension and the complexity of the objective function, is available, partitioned or local studies are beneficial. In this work we propose a new method called local active subspaces (LAS), which explores the synergies of active subspaces with supervised clustering techniques in order to perform a more efficient dimension reduction in the parameter space for the design of accurate response surfaces. We also developed a procedure to exploit the local active subspace information for classification tasks. Using this technique as a preprocessing step onto the parameter space, or output space in case of vectorial outputs, brings remarkable results for the purpose of surrogate modelling.

## Contents

<b>1</b>	<b>Introduction</b>	<b>2</b>
<b>2</b>	<b>Active subspaces for parameter space reduction</b>	<b>3</b>
<b>3</b>	<b>Localized parameter space reduction</b>	<b>3</b>
3.1	K-means clustering . . . . .	3
3.2	K-medoids clustering with active subspaces-based metric . . . . .	4
3.3	Hierarchical top-down clustering . . . . .	5
3.3.1	Ridge approximation with hierarchical clustering and active subspaces . . .	5
3.3.2	Implementation of hierarchical clustering with active subspaces . . . . .	9
<b>4</b>	<b>Classification with local active subspace dimension</b>	<b>10</b>
<b>5</b>	<b>Numerical results</b>	<b>12</b>
5.1	Some illustrative bidimensional examples . . . . .	13
5.1.1	Quartic function . . . . .	13
5.1.2	Radial symmetric cosine . . . . .	15
5.2	High-dimensional datasets . . . . .	16
5.2.1	Multi-dimensional hyper-paraboloid . . . . .	16
5.2.2	Ebola epidemic model . . . . .	17
5.3	Datasets with vectorial outputs . . . . .	17
5.3.1	Poisson equation with random diffusivity . . . . .	18
5.3.2	Shape design of an airfoil . . . . .	20

---

\*francesco.romor@sissa.it

†marco.tezzele@sissa.it

‡gianluigi.rozza@sissa.it

## 1 Introduction

Parameter space reduction is a rapidly growing field of interest which plays a key role in fighting the curse of dimensionality. The need of reducing the number of design inputs is particularly important in engineering for advanced CFD simulations to model complex phenomena, especially in the broader context of model order reduction [30] and industrial numerical pipelines [32, 31, 37].

Active subspaces [6] is one of the most used techniques for linear reduction in input spaces. It has been proved useful in many numerical tasks such as regression, using a multi-fidelity data fusion approach with a surrogate model built on top of the AS as low-fidelity model [29]; shape optimization [21, 39] and a coupling with the genetic algorithm to enhance its performance [10, 8]; or inverse problems [44]. It has also been used to enhance classical model order reduction techniques such as POD-Galerkin [36], and POD with interpolation [9]. Other attempts towards nonlinear parameter space reduction have been proposed recently: kernel-based active subspaces [27], nonlinear level-set learning [45], and active manifold [4] are the most promising.

In this work we propose a new local approach for parameter space dimensionality reduction for both regression and classification tasks, called Local Active Subspaces (LAS). Other methods have been developed in the last years exploiting the localization idea. We mention localized slice inverse regression (LSIR) [42] which uses local information of the slices for supervised regression and semi-supervised classification. LSIR improves local discriminant information [15] and local Fischer discriminant analysis [34] with more efficient computations for classification problems. The main difference between slice inverse regression (SIR) [19] and AS is in the construction of the projection matrix. While SIR needs the elliptic assumption, AS exploits the gradients of the function of interest with respect to the input parameters.

From a wider point of view, there is an analogy between local parameter space reduction and local model order reduction. With the latter, we mean both a spatial domain decomposition approach for model order reduction of parametric PDEs in a spatial domain  $\Omega \subset \mathbb{R}^d$  and a local reduction approach in the parameter space. As representative method for the first paradigm we report the reduced basis element method [20], which combines the reduced basis method in each subdomains with a mortar type method at the interfaces. For the second approach we cite the interpolation method in the Grassmann manifold of the reduced subspaces [2]; in particular in [7] the K-medoids clustering algorithm with Grassmann metric is applied to the discrete Grassmann manifold of the training snapshots as a step to perform local model order reduction.

Similarly, in our work we do not simply apply a clustering technique to preprocess the input data, we propose a supervised metric induced by the presence of a global active subspace. The directions individuated by local active subspaces are locally linear, and they better capture the latent manifold of the target function. Moreover the effectiveness of the chosen metric is linked to the fact that normally we do not employ the optimal profile (which is a conditioned random variable and in this sense nonlinear) for the construction of response surfaces on the active subspace, and with the use of clustering with AS-based metric we try to reduce this approximation error. Essentially, we are splitting the response surface design transversally with respect to the active subspace, which, having in mind that the optimal profile is obtained integrating out the inactive variable, means splitting the integral in a sum of terms associated to the number of clusters.

This work is organized as follows: in section 2 we briefly review the active subspaces method, in section 3 we introduce the clustering algorithms used and the supervised distance metric based on the presence of a global active subspace, focusing on the construction of response surfaces and providing theoretical results. In section 4 we present the algorithms to exploit LAS for classification. We provide extensive numerical results in section 5 from simple illustrative bidimensional dataset to high-dimensional scalar and vector-valued functions. Finally in section 6 we draw some conclusions and future perspectives.

## 2 Active subspaces for parameter space reduction

Active subspaces (AS) [6] is a linear technique to unveil a lower dimensional structure of a function of interest  $f$ . Through spectral considerations about the second moment matrix of  $\nabla f$ , it identifies a set of linear combinations of the input parameters along which  $f$  varies the most. This can also be seen in the context of ridge approximation [26].

Let us introduce the input domain  $\mathcal{X} \subset \mathbb{R}^n$ . Usually it is an  $n$ -dimensional hyperrectangle. To compute the active subspace of a real-valued function  $f$  defined in  $\mathcal{X}$  we are going to rescale the input parameters  $\mathbf{X}$  to  $[-1, 1]^n$ . An extension to vector-valued functions has been presented in [43] and extended for kernel-based AS in [27]. Even if in this section we focus only on scalar functions, the following considerations can be carried over to the multivariate case without too much effort.

Let  $\Sigma$  be the second moment matrix of  $\nabla f$  defined as

$$\Sigma := \mathbb{E} [\nabla_{\mathbf{x}} f \nabla_{\mathbf{x}} f^T] = \int (\nabla_{\mathbf{x}} f)(\nabla_{\mathbf{x}} f)^T d\boldsymbol{\mu}, \quad (1)$$

where  $\mathbb{E}$  denotes the expected value,  $\nabla_{\mathbf{x}} f = \nabla f(\mathbf{x}) = \left[ \frac{\partial f}{\partial x_1}, \dots, \frac{\partial f}{\partial x_n} \right]^T$  is the column vector of partial derivatives of  $f$ , and  $\boldsymbol{\mu}$  is a probability measure on some  $\sigma$ -algebra on  $\mathcal{X}$ . Its real eigenvalue decomposition reads:

$$\Sigma = \mathbf{W} \boldsymbol{\Lambda} \mathbf{W}^T. \quad (2)$$

We can retain only the most energetic eigenpairs by looking at the spectral decay of the matrix  $\Sigma$ . The number  $r$  of eigenpairs we select is the active subspace dimension, and the span of the corresponding eigenvectors defines the active subspace. The partition is the following

$$\boldsymbol{\Lambda} = \begin{bmatrix} \boldsymbol{\Lambda}_1 & \\ & \boldsymbol{\Lambda}_2 \end{bmatrix}, \quad \mathbf{W} = [\mathbf{W}_1 \quad \mathbf{W}_2], \quad (3)$$

where  $\boldsymbol{\Lambda}_1 = \text{diag}(\lambda_1, \dots, \lambda_r)$ , and  $\mathbf{W}_1$  contains the first  $r$  eigenvectors arranged by columns. With this matrix we can project the input parameters onto the active subspace, and its orthogonal complement, that is the inactive subspace, as follows:

$$\mathbf{Y} = P_r(\mathbf{X}) = \mathbf{W}_1 \mathbf{W}_1^T \mathbf{X} \in \mathbb{R}^n, \quad \mathbf{Z} = (I - P_r)(\mathbf{X}) = \mathbf{W}_2 \mathbf{W}_2^T \mathbf{X} \in \mathbb{R}^n. \quad (4)$$

The selection of the active subspace dimension  $r$  can be set a priori, or by looking at the presence of a spectral gap [6], or by imposing a cumulative energy threshold for the eigenvalues.

## 3 Localized parameter space reduction

Sometimes we do not have *a priori* knowledge about the target function's behaviour in a particular parameter space region. So it is difficult to properly set the parameters range. In these cases a preprocessing of the data using a clustering technique could be highly beneficial. With a clustering of the input parameters we can treat each subregion separately, and thus being able to better capture the target function's variability. This is always true for any function of interest, but for functions with global lower intrinsic dimensionality we can exploit such structure to enhance the clustering. To this end we propose a new distance metric for K-medoids and hierarchical top-down clustering methods which exploits the global active subspace of the target function.

By applying AS on each cluster we find the optimal rotation of the corresponding subregion of the input domain, which aligns the data along the active subspace of a given dimension.

In this section we review two of the main partitioning methods [14] such as K-means, K-medoids, and the hierarchical top-down clustering technique [18, 23]. We are going to use K-means as the baseline since the input parameter space is assumed to be an hyperrectangle — as is done in every practical case — and we do not expect samples which are highly concentrated in a specific subregion.

### 3.1 K-means clustering

Let  $\{x_i\}_{i=1}^N$  be a set of  $N$  samples in  $\mathbb{R}^{N_F}$ , where  $N_F$  denotes the number of features. The K-means algorithm divides this set into  $K$  disjoint clusters  $S = \{S_j\}_{j=1}^K$ , with  $S_l \cap S_m = \emptyset$  for

$1 \leq l, m \leq K$  and  $l \neq m$ . The partitioning quality is assessed by a function which aims for high intracluster similarity and low intercluster similarity. For K-means this is done by minimizing the total within-cluster sum-of-squares criterion  $W_T$ , which reads as

$$W_T(S) := \sum_{j=1}^K W(S_j) = \sum_{j=1}^K \sum_{x_i \in S_j} \|x_i - c_j\|_{L^2}^2, \quad (5)$$

where  $c_j$  is the centroid describing the cluster  $S_j$ . A centroid of a cluster is defined as the mean of all the points included in that cluster. This means that the centroids are, in general, different from the samples  $x_i$ .

K-means is sensitive to outliers, since they can distort the mean value of a cluster and thus affecting the assignment of the rest of the data. Algorithm 1 shows the pseudo-code of the K-means algorithm.

---

**Algorithm 1:** K-means algorithm.

---

**input** : set of samples  $\{x_i\}_{i=1}^N \in \mathbb{R}^{N_F}$ ,  
number of clusters  $K$

**output:** set of clusters  $S = \{S_j\}_{j=1}^K$

1 select initial cluster centroids.

2 **repeat**

3     | assign each sample to its closest centroid using the Euclidean distance.

4     | update the centroid of each cluster.

5 **until** *criterion  $W_T$  of equation (5) is minimized.*

---

### 3.2 K-medoids clustering with active subspaces-based metric

In order to overcome some limitations of the K-means algorithm, such as sensitivity to outliers, we can use K-medoids clustering technique [18, 25, 33, 22]. It uses an actual sample as cluster representative (i.e. medoid) instead of the mean of the samples within the cluster.

Following the notation introduced in the previous section, let  $m_j$  be the medoid describing the cluster  $S_j$ . The partitioning method is performed by minimizing the sum of the dissimilarities between the samples within a cluster and the corresponding medoid. To this end an absolute-error criterion  $E$  is used, which reads as

$$E(S) := \sum_{j=1}^K E(S_j) = \sum_{j=1}^K \sum_{x_i \in S_j} \|x_i - m_j\|. \quad (6)$$

By looking at the formula above it is clear that the use of a data point to represent each cluster's center allows the use of any distance metric for clustering. We remark that the choice of the Euclidean distance does not produce the same results as K-means because of the different references representing the clusters.

We propose a new supervised distance metric inspired by the global active subspace of the function  $f$  we want to approximate. We define a scaled  $L^2$  norm using the eigenpairs of the second moment matrix of  $\nabla f$ , which is the matrix from which we calculate the global active subspace:

$$\|x_i - x_j\|_{\Lambda} = \sqrt{(x_i - x_j)^T \mathbf{W} \Lambda^2 \mathbf{W}^T (x_i - x_j)}, \quad (7)$$

where  $\Lambda$  stands for the diagonal matrix with entries the eigenvalues of equation (1), and  $\mathbf{W}$  is the eigenvectors matrix from equation (2). As we are going to show in section 5 this new metric allows a better partitioning both for regression and classification tasks because of it exploits both global and local informations. For stronger insights about the heuristic behind, see remark 7.

To actually find the medoids, the partitioning around medoids (PAM) algorithm [18] is used. It uses a greedy approach after the initial selection of the medoids, also called representative objects. They are changed with a non-representative object, i.e. one of the remaining samples, if it would

---

**Algorithm 2:** K-medoids algorithm with AS metric.

---

**input** : set of samples  $\{x_i\}_{i=1}^N \in \mathbb{R}^{N_F}$ ,  
number of clusters  $K$ ,  
distance metric  $d$  defined in equation (7)

**output:** set of clusters  $S = \{S_j\}_{j=1}^K$

- 1 select initial cluster medoids.
- 2 **repeat**
- 3     assign each sample to its closest medoid using the distance metric  $d$ .
- 4     randomly select  $K$  non-representative objects.
- 5     swap the medoids with the new selected objects by minimizing equation (6).
- 6 **until** clustering quality converges.

---

improve the clustering quality. This iterative process of replacing the medoids by other objects continues until the quality of the resulting clustering cannot be improved by any replacement. Algorithm 2 illustrates this approach with pseudo-code.

### 3.3 Hierarchical top-down clustering

In this section we present Hierarchical top-down clustering with Active Subspaces (HAS), a variant of the previous methodologies with hierarchical top-down clustering [18, 23], that exploits, as previously, the additional information from the active subspace.

In top-down hierarchical clustering, at each iteration the considered clusters, starting from the whole dataset, are split further and further based on some refinement criterion, until convergence. A nice feature of hierarchical clustering algorithms, with respect to K-means and K-medoids, is that the number of clusters can be omitted. Moreover, stopping at the first refinement and forcing the total number of clusters, HAS can be seen as a generalization of the previous methods: for this reason we wanted to make the implementation consistent with K-means and K-medoids with AS induced metric as close as possible, as shown in the numerical results in section 5.

Pushing further the potential of clustering algorithms applied to local dimension reduction in the parameter space, HAS is a versatile clustering method that takes into account the variability of the AS dimension along the parameter space. The price paid for this is the overhead represented by the tuning of some hyper-parameters introduced later in section 3.3.2.

#### 3.3.1 Ridge approximation with hierarchical clustering and active subspaces

Before presenting the algorithm and the numerical results, some straightforward theoretical considerations linked to the theory of ridge approximation with active subspaces [6, 43] are due. We will consider scalar outputs  $f$  but the following statements can be extended to vector-valued outputs.

**Definition 1** (Local ridge approximation with active subspaces). *Given a partition of the domain  $\mathcal{P} := \{S_i\}_{i \in \{1, \dots, d\}}$  and a map  $r : \mathcal{P} \rightarrow \{1, \dots, n_r\}$ ,  $n_r \ll n$  representing the local reduced dimension, the local ridge approximation with active subspaces of  $(f, \boldsymbol{\mu})$  is the function  $R_{AS}(r, f, \boldsymbol{\mu}) : \mathcal{X} \subset \mathbb{R}^n \rightarrow \mathbb{R}$  that is defined locally for every  $S_i \in \mathcal{P}$  as*

$$g|_{S_i} = \mathbb{E}_{\boldsymbol{\mu}_i} [f|_{P_{r(S_i),i}}] \circ P_{r(S_i),i} \quad (8)$$

where  $\boldsymbol{\mu}_i := (1/\boldsymbol{\mu}(S_i)) \cdot \boldsymbol{\mu}|_{S_i} \mathbb{R}^n$ , and  $P_{r,i} : S_i \subset \mathbb{R}^n \rightarrow \mathbb{R}^n$  is the orthogonal projector with rank  $r$  that satisfies the minimization problem

$$P_{r,i} = \underset{\substack{P^2=P, P=P^T, \\ \text{rank}(P)=r}}{\text{argmin}} \mathbb{E}_{\boldsymbol{\mu}_i} \|(Id - P)\nabla f\|^2 = \underset{\substack{P^2=P, P=P^T, \\ \text{rank}(P)=r}}{\text{argmin}} \text{tr}((Id - P)\mathbb{E}_{\boldsymbol{\mu}_i} [\nabla f \otimes \nabla f](Id - P)). \quad (9)$$

The above minimization problem is an adaptation from Proposition 2.6 of [43]. With this definition we can state the problem of local ridge approximation with active subspaces.

**Problem 1** ( $(\mathcal{P}, r)$  minimizers of ridge approximation error). *Find the partition  $\mathcal{P}$  of the domain  $\mathcal{X} \subset \mathbb{R}^n$  and the local reduced dimension map  $r : \mathcal{P} \rightarrow \{1, \dots, n_r\}$ ,  $n_r \ll n$ , such that the  $L^2$ -error between the objective function  $f$  and its local ridge approximation with active subspaces is*

minimized. Assuming that the subspace Poincaré inequality [24] is valid also for  $(f, \boldsymbol{\mu})$  restricted to the elements of the partition  $\mathcal{P}$ , a straightforward bound is obtained applying the Poincaré inequality for every element of the partition

$$\begin{aligned} \mathbb{E}_{\boldsymbol{\mu}} [\|f - R_{AS}(r, f)\|^2] &= \sum_{S_i \in \mathcal{P}} \mathbb{E}_{\boldsymbol{\mu}} [\|f|_{S_i} - \mathbb{E}_{\boldsymbol{\mu}_i}[f|_{P_r(S_i, S_i)}] \circ P_r(S_i, S_i)\|^2] \\ &\lesssim \sum_{S_i \in \mathcal{P}} \mathbb{E}_{\boldsymbol{\mu}} [\|(Id - P_r(S_i, S_i))^T \nabla f\|^2] \end{aligned}$$

To state problem 1 we made an assumption about the Poincaré subspace inequality that in general is not satisfied by any probability measure  $\boldsymbol{\mu}$  chosen.

**Remark 1** (Subspace Poincaré inequality). The probabilistic Poincaré inequality for conditional probability densities or subspace Poincaré inequality [24] is valid at least for the following classes of absolutely continuous probability densities  $\boldsymbol{\mu}$  with p.d.f.  $\rho$ .

**Assumption 1.** The p.d.f  $\rho : \mathcal{X} \subset \mathbb{R}^n \rightarrow \mathbb{R}$  satisfies one of the following:

1.  $\mathcal{X}$  is bounded connected open with Lipschitz boundary,  $\rho$  is the uniform density distribution.
2.  $\mathcal{X}$  is convex and bounded,  $\exists \delta, D > 0 : 0 < \delta \leq \|\rho(\mathbf{x})\|_{L^\infty} \leq D < \infty, \forall \mathbf{x} \in \mathcal{X}$ ,
3.  $\mathcal{X} = \mathbb{R}^n$ ,  $\rho(\mathbf{x}) \sim \exp(-V(\mathbf{x}))$  where  $V : \mathbb{R}^n \rightarrow (-\infty, \infty], V \in \mathcal{C}^2$  is  $\alpha$ -uniformly convex,

$$\mathbf{u}^T \text{Hess}(V(\mathbf{x})) \mathbf{u} \geq \alpha \|\mathbf{u}\|_2^2, \quad \forall \mathbf{x}, \mathbf{u} \in \mathbb{R}^n, \quad (10)$$

where  $\text{Hess}(V(\mathbf{x}))$  is the Hessian of  $V(\mathbf{x})$ .

4.  $\mathcal{X} = \mathbb{R}^n$ ,  $\rho(\mathbf{x}) \sim \exp(-V(\mathbf{x}))$  where  $V$  is a convex function. In this case we require also  $f$  Lipschitz continuous.

The last class of p.d.f. provides a weaker bound (Lemma 4.3, [24]) on the ridge approximation error. For the previous classes  $i \in \{1, 2, 3, 4\}$  of p.d.f. an upper bound of the Poincaré constant  $C_{P,i}$  is also provided:

$$C_{P,1} = C_{P,1}(\Omega), \quad C_{P,2} = \frac{D \text{diam}(\mathcal{X})}{\pi \delta}, \quad C_{P,3} = \frac{1}{\alpha}, \quad (11)$$

while the upper bound for  $C_{P,4}$  requires the definition of other quantities and is proved in Lemma 4.4 [24]. These results are useful to assess what properties the elements of the partition  $\mathcal{P} = \{S_i\}_{i \in \{1, \dots, d\}}$  should satisfy in order for the subspace Poincaré inequality to be valid and thus for the bound in remark 2 to be applied recursively with respect to the refinement levels. In the numerical experiments we are going to present, the partition  $\mathcal{P} = \{S_i\}_{i \in \{1, \dots, d\}}$  is defined by the decision boundaries of the clustering algorithm chosen.

For the moment we will consider the local reduced dimension map  $r$  constant and in general the codomain of  $r$  is a subset of  $\{1, \dots, n_r\}$ ,  $n_r \ll n$ .

The previous bound suggests that a good indicator for refinement could be represented by the residual eigenvalues of the local correlation matrix. We also have the following immediate result that hints to indefinitely many successive refinements to lower the  $L^2$ -error.

**Remark 2** (Relationships between the upper bounds of consecutive refinements). Considering the sum over the number of refined clusters  $cl \in \{1, \dots, d\}$  we have that

$$\int_{\mathcal{X}} \|(Id - P_r^T) \nabla f\|^2 d\boldsymbol{\mu} = \sum_{cl=1}^d \int_{S_{cl} \subset \mathcal{X}} \|(Id - P_r^T) \nabla f\|^2 d\boldsymbol{\mu} \geq \sum_{cl=1}^d \int_{S_{cl} \subset \mathcal{X}} \|(Id - P_{r,cl}^T) \nabla f\|^2 d\boldsymbol{\mu}, \quad (12)$$

since the projectors  $\{P_{r,cl}\}_{cl \in \{1, \dots, d\}}$  are the minimizers of

$$P_{r,cl} = \underset{\substack{P^2=P, P=P^T, \\ \text{rank}(P)=r}}{\text{argmin}} \int_{S_{cl} \subset \mathcal{X}} \|(Id - P^T) \nabla f\|^2 d\boldsymbol{\mu}. \quad (13)$$

The RHS of equation (12) can be used as indicator for refinement. We remark that since the refinements increase the weight decay of the eigenvalues in the RHS of equation (12), the choice of the dimension of the active subspace may be shifted towards lower values, as we are going to show in the numerical experiments, in section 5.

Unfortunately, the minimizers of the ridge approximation error and of the upper bound are not generally the same. There is a counterexample in [43]. We start from this counterexample to show that in general the  $L^2$ -error of the local ridge approximation does not decrease between consequent refinements, even if the indicator from the RHS of equation (12) does, as stated in the previous remark.

**Corollary 1** (Counterexample for indefinite refinement as optimal clustering criterion). *Let  $\mathcal{P} = \{A, B, C\}$  be a partition of  $\mathcal{X} = [-1, 1]^2$  such that  $A = [-1, \epsilon] \times [-1, 1]$ ,  $B = [-\epsilon, \epsilon] \times [-1, 1]$ , and  $C = [\epsilon, 1] \times [-1, 1]$ . Let  $\mu$  be the uniform probability distribution on  $\mathcal{X}$ . The objective function we want to approximate is*

$$f : \mathcal{X} \subset \mathbb{R}^2 \rightarrow \mathbb{R}, \quad f = \begin{cases} x_1 + \epsilon, & \mathbf{x} \in A, \\ x_1(x_1 + \epsilon)(x_1 - \epsilon) \cos(\omega x_2), & \mathbf{x} \in B, \\ x_1 - \epsilon, & \mathbf{x} \in C, \end{cases} \quad (14)$$

with local reduced dimension map  $r(A) = r(B) = r(C) = 1$ . There exist  $\epsilon > 0, \omega > 0$ , such that

$$\mathbb{E}_\mu [\|f - R_{AS}(r, f, \mu)\|^2] \geq \mathbb{E}_\mu [\|f - \mathbb{E}_\mu [f|P_{1,\mathcal{X}}] \circ P_{1,\mathcal{X}}\|^2],$$

where  $P_{1,\mathcal{X}}$  is the optimal projector on the whole domain  $\mathcal{X}$  with one-dimensional active subspace.

*Proof.* The proof is reported in appendix A.  $\square$

The heuristic behind the previous proof rests on the fact that ridge approximation with active subspaces performs poorly when the objective function has a high variation. The counterexample is valid whenever the global projector  $P_{1,\mathcal{X}}$  is the minimizer of a local  $L^2$  ridge approximation error for which the minimizer of the gradient-based indicator in equation (12) does not coincide. This leaves us with an indicator in equation (12) that does not guarantee a non increasing  $L^2$ -error decay for subsequent refinements.

We conclude the section with some remarks about the response surface design through the ridge approximation with active subspaces.

**Remark 3** (Approximation of the optimal profile). In practice we do not consider the optimal profile  $h(y) = \mathbb{E}_\mu [f|\sigma(P_r)](y)$  but we employ the approximation  $h(y) = f(P_r, \mathbf{x})$ . The reason lies on the fact that to approximate the optimal profile at the value  $\{y_i\}_i$ , additional samples from the conditional distribution  $p(z|y_i = P_r, \mathbf{x})$  must be obtained; even if the accuracy of the ridge approximation could benefit from it, this is not always possible in practice because of the difficulty to sample from the conditional distribution or because of computational budget constraints.

If the data is split in training, validation, and test set, the local  $R^2$  score on the validation set can be used as indicator for refinement.

**Remark 4** (Estimator based on local  $R^2$  scores). The  $R^2$  score of a single cluster can be written with respect to the  $R^2$  scores  $\{R_l^2\}_{l \in \{1, \dots, d\}}$  relative to the clusters of the subsequent refinement. Let the sum be over the refinement clusters  $l \in \{1, \dots, d\}$ , we have

$$\begin{aligned} R^2 &= 1 - \frac{\mathbb{E}[\|f - \mathbb{E}[f|P_r] \circ P_r\|^2]}{\text{Var}(f)} = 1 - \sum_{l=1}^d \frac{\mathbb{E}[\|f|_{S_l} - \mathbb{E}[f|P_{r,l}] \circ P_{r,l}\|^2]}{\text{Var}(f)} \\ &= 1 - \sum_{l=1}^d \frac{\text{Var}(f|_{S_l})}{\text{Var}(f)} \cdot \frac{\mathbb{E}[\|f|_{S_l} - \mathbb{E}[f|P_{r,l}] \circ P_{r,l}\|^2]}{\text{Var}(f|_{S_l})} = 1 - \sum_{l=1}^d \frac{\text{Var}(f|_{S_l})}{\text{Var}(f)} \cdot (1 - R_l^2), \end{aligned} \quad (15)$$

which, substituting with the empirical variance, becomes

$$R_{\text{emp}}^2 = 1 - \sum_{l=1}^d \frac{\text{Var}_{\text{emp}}(f|_{S_l})}{\text{Var}_{\text{emp}}(f)} \cdot (1 - R_{\text{emp};l}^2) \cdot \frac{N_l - 1}{N - 1}, \quad (16)$$

where  $R_{\text{emp};l}^2$  is the empirical local  $R^2$  score relative to cluster number  $l$ . The definition can be extended for component-wise vector-valued objective functions  $f$ . The numerical results shown in section 5 consider the mean  $R^2$  score along the components when the output is vectorial.

In practice every mean is approximated with simple Monte Carlo, and without the number of training samples increasing, the confidence on the approximation is lower and lower, the more the domain is refined. This is taken into consideration while clustering: the procedure balances the error from the poor Monte Carlo approximation with the generally (see corollary 1) higher accuracy of the subsequent refinement.

The following remark clarifies the link between the number of Monte Carlo samples, the numerical method chosen for the discretization of the integral  $\mathbb{E}_{\mu} [\nabla f \otimes \nabla f]$ , and the approximation of the active subspace. For example for deterministic models, one could employ the more efficient Sobol sequences or a Latin hypercube sampling; if  $f$  is more regular and the parameter space dimension is not too high one could employ tensor product Gauss quadrature rule. See for example [35].

**Remark 5** (Generalization of the upper bound on the approximation of the active subspace). We want to make some brief considerations about the accuracy of the active subspace as eigen subspace of the correlation matrix approximated with Monte Carlo. If we use the notation  $W_1 \in \mathbb{R}^{n \times r}$ ,  $W_2 \in \mathbb{R}^{n \times (n-r)}$  for the active and inactive subspaces (i.e.  $P_r = W_1 W_1^T$ ,  $Id - P_r = W_2 W_2^T$ ) and  $\hat{W}_1 \in \mathbb{R}^{n \times r}$ ,  $\hat{W}_2 \in \mathbb{R}^{n \times (n-r)}$  for the approximated active and inactive subspaces), we can bound the approximation error as done by Constantine in [6]: assuming  $f$  Lipschitz continuous, with high probability the following inequality is valid,

$$\text{dist}(\text{Im}(W_1), \text{Im}(\hat{W}_1)) \lesssim \frac{4L\sqrt{n}(\log(n))^{\frac{1}{2}}}{N^{\frac{1}{2}}\lambda_1(\lambda_r - \lambda_{r+1})}, \quad (17)$$

where  $L$  is the Lipschitz constant of  $f$ ,  $\{\lambda_1, \dots, \lambda_n\}$  are the non-negative eigenvalues of  $\mathbb{E}_{\mu_i} [\nabla f \otimes \nabla f]$  ordered decreasingly, and  $N$  is the number of Monte Carlo samples.

The bound in equation (17) is obtained from Corollary 3.8 and Corollary 3.10 in [6]. It is founded on a matrix Bernstein inequality for a sequence of random uniformly bounded matrices (Theorem 6.1, [40]) and on the Corollary 8.1.11 from [12] that holds a bound on the sensitivity of perturbation of an invariant subspace. We report this last result for completeness, stated as Lemma 3.9 from [6]:

**Theorem 1** (Theorem 8.1.11 from [12], Lemma 3.9 from [6]). *Let  $C$  and  $\hat{C} = C + E$  be symmetric  $n \times n$  matrices with respective eigenvalues  $\lambda_1, \dots, \lambda_n$  and  $\hat{\lambda}_1, \dots, \hat{\lambda}_n$  and eigenvector matrices*

$$W = [W_1 \ W_2], \quad \hat{W} = [\hat{W}_1 \ \hat{W}_2], \quad (18)$$

as defined previously. If  $\lambda_r > \lambda_{r+1} + 1$  and

$$\|E\|_F \leq \frac{\lambda_r - \lambda_{r+1}}{5}, \quad (19)$$

then

$$\text{dist}(\text{Im}(W_1), \text{Im}(\hat{W}_1)) \leq \frac{4\|W_2^T E W_1\|_F}{\lambda_r - \lambda_{r+1}} \leq \frac{4\|E\|_F}{\lambda_r - \lambda_{r+1}}. \quad (20)$$

From this result, a bound on the approximation error of the active subspace  $W_1$  can be obtained expliciting  $\|W_2^T E W_1\|_F$  with respect to the chosen numerical method for the discretization  $\hat{C}$  of the integral  $C = \mathbb{E}_{\mu_i} [\nabla f \otimes \nabla f]$ : in [6] this has been done for the Monte Carlo method. In practice we could use quasi Monte Carlo sampling methods with Halton or Sobol sequences [35], since

$$\begin{aligned} \|W_2^T E W_1\|_F &\leq \sqrt{r(n-r)} \|W_2^T E W_1\|_{\max} \lesssim \sqrt{r(n-r)} D^*({x_i}_i) \cdot \max_{i,j \in \{1, \dots, n\}} (V^{\text{HK}}(\nabla f_i \nabla f_j)) \\ &\lesssim 2\sqrt{r(n-r)} D^*({x_i}_i) \cdot \max(|f|) \cdot \max_{i \in \{1, \dots, n\}} (V^{\text{HK}}(\nabla f_i)) \\ &\lesssim 2\sqrt{r(n-r)} \cdot \max_{i \in \{1, \dots, n\}} (V^{\text{HK}}(\nabla f_i)) \frac{\log(N)^n}{N}, \end{aligned}$$

where  $V^{\text{HK}}$  is the Hardy–Krause variation and  $D^*({x_i}_i)$  is the star discrepancy of the quasi random sequence  $\{x_i\}_i$ . For the above result we have imposed  $\mathcal{X} = [0, 1]^n$  but it can be extended to different domains [3]. Thus we obtain the bound

$$\text{dist}(\text{Im}(W_1), \text{Im}(\hat{W}_1)) \lesssim \frac{4\|W_2^T E W_1\|_F}{\lambda_r - \lambda_{r+1}} \lesssim \frac{8L\sqrt{r(n-r)} \cdot \max_{i \in \{1, \dots, n\}} (V^{\text{HK}}(\nabla f_i))}{\lambda_r - \lambda_{r+1}} \cdot \frac{\log(N)^n}{N}. \quad (21)$$

Other numerical integration rules can be chosen so that different regularity conditions on the objective function may appear on the upper bound of the error, as the Lipschitz constant on equation (17) or the Hardy–Krause variation on equation (21). For example, for tensor product quadrature formulae [35], if the regularity of  $f$  is  $\mathcal{C}^s$  we have generally,

$$\text{dist}(\text{Im}(W_1), \text{Im}(\hat{W}_1)) \lesssim \frac{4\|W_2^T E W_1\|_F}{\lambda_r - \lambda_{r+1}} \lesssim \frac{4\sqrt{r(n-r)}}{N^{s/n}(\lambda_r - \lambda_{r+1})}, \quad (22)$$

or for Smolyak’s sparse quadrature rule [35],

$$\text{dist}(\text{Im}(W_1), \text{Im}(\hat{W}_1)) \lesssim \frac{4\|W_2^T E W_1\|_F}{\lambda_r - \lambda_{r+1}} \lesssim \frac{4\sqrt{r(n-r)} (\log N)^{(n-1)(r+1)}}{N^s(\lambda_r - \lambda_{r+1})}. \quad (23)$$

For high-dimensional datasets and  $f$  less regular, the estimate 17 is the sharpest.

### 3.3.2 Implementation of hierarchical clustering with active subspaces

A schematic representation of the procedure of top-down clustering is reported in algorithm 3. The design is straightforward and it employs a tree data structure that assigns at each node a possible clustering of the whole dataset: consequent refinements are represented by children nodes down until the leaves of the tree, that represent the final clusters.

**Remark 6** (Normalization of the clusters at each refinement iteration). Each cluster, at every refinement step, is normalized uniformly along dimensions onto the hyper-cube domain  $[-1, 1]^n$ . Another possible choice for normalization is standardization, centering the samples with their mean and dividing them by their standard deviation.

---

**Algorithm 3:** Hierarchical top-down algorithm.

---

**input** : set of samples  $\mathbf{S} = \{x_i\}_{i=1}^N \in \mathbb{R}^{N \times F}$ ,  
number of clusters per tree refinement level  $\mathbf{K}$ ,  
range of number of children  $\{\mathbf{n}_{\mathbf{m}}^{\mathbf{h}}, \mathbf{n}_{\mathbf{m}}^{\mathbf{b}}\}$ ,  
minimum number of elements in a cluster  $\mathbf{n}_{\mathbf{b}}$ ,  
indicator for refinement  $\mathbf{I}$ ,  
distance metric  $\mathbf{d}$ ,  
minimum and maximum dimension of the active subspace  $\mathbf{r}_{\mathbf{m}}, \mathbf{r}_{\mathbf{m}}$ ,  
score tolerance  $\epsilon$ .

**output:** refinement tree  $T = S(S_1(S_{k+1}(\dots, (S_{\text{leaf},1}), \dots), \dots), \dots, S_k(\dots))$ , with  
 $k \in \{\mathbf{n}_{\mathbf{m}}^{\mathbf{h}}, \dots, \mathbf{n}_{\mathbf{m}}^{\mathbf{b}}\}$ .

- 1 add the initial cluster  $S$  to FIFO queue  $q = \{S\}$ .
- 2 **while**  $q \neq \emptyset$  **do**
- 3     take  $\mathbf{S}_j$ , the first element from queue  $q$ .
- 4     apply the refinement function in algorithm 4 to  $\mathbf{S}_j$  in order to get the outputs  $\{S_i\}_i$ .
- 5     add  $\{S_i\}_i$  to the queue  $q$ .
- 6     **if** (the score tolerance  $\epsilon$  is reached
- 7         **or** the minimum number of elements in a cluster  $n_{el}$  is reached in the next iteration
- 8         **or** the maximum number of clusters  $\mathbf{K}$  is reached in the next iteration) **then**
- 9         | **break**

---

The procedure depends on many parameters that have to be tuned for the specific case or depend *a priori* on the application considered: the maximum number of clusters, the minimum and maximum number of children nodes, the tolerance for the score on the whole domain, the minimum and maximum dimension of the active subspace, and the minimum number of elements ( $el$ ) of each cluster (usually  $el > r$ , where  $r$  is the local AS dimension).

More importantly the method is versatile for the choice of clustering criterion, indicator for refinement, and regression method. In the following sections we will consider K-means and K-medoids with the active subspaces distance as clustering criterion (see section 3.2), but other clustering algorithms could in principle be applied at each refinement.

---

**Algorithm 4:** Refinement function.

---

**input** : cluster  $\mathbf{S} = \{x_i\}_{i=1}^N \in \mathbb{R}^{N_F}$ ,  
number of clusters per tree refinement level  $\mathbf{K}$ ,  
range of number of children  $\{\mathbf{n}_{\mathbf{m}}^{\mathbf{h}}, \mathbf{n}_{\mathbf{m}}^{\mathbf{h}}\}$ ,  
minimum number of elements in a cluster  $\mathbf{n}_{\mathbf{b}}$ ,  
indicator for refinement  $\mathbf{I}$ ,  
distance metric  $\mathbf{d}$ ,  
minimum and maximum dimension of the active subspace  $\mathbf{r}_{\mathbf{m}}, \mathbf{r}_{\mathbf{m}}$ .

**output:**  $\{S_j\}_{j=1}^{\mathbf{n}_{\mathbf{m}}^{\mathbf{h}}}$ , the children of cluster  $\mathbf{S}$ , with  $\mathbf{n}^{\mathbf{h}} \in \{\mathbf{n}_{\mathbf{m}}^{\mathbf{h}}, \dots, \mathbf{n}_{\mathbf{m}}^{\mathbf{h}}\}$ .

- 1 set best score to  $b = 0$ .
- 2 **foreach**  $\mathbf{n}^{\mathbf{h}}$  from  $\mathbf{n}_{\mathbf{m}}^{\mathbf{h}}$  to  $\mathbf{n}_{\mathbf{m}}^{\mathbf{h}}$  **do**
- 3     apply the chosen clustering algorithm (e.g. K-medoids) with  $\mathbf{n}^{\mathbf{h}}$  clusters and metric  $\mathbf{d}$  to obtain the clusters  $\{S_j\}_j^{\mathbf{n}^{\mathbf{h}}}$ .
- 4     evaluate the estimator of the error  $\mathbf{I}$  for the refinement  $\{S_j\}_j$ , taking also into account the minimum and maximum reduced dimensions  $\mathbf{r}_{\mathbf{m}}, \mathbf{r}_{\mathbf{m}}$ .
- 5     **if**  $\mathbf{I} > b$  **and** the minimum number of elements  $\mathbf{n}_{\mathbf{b}}$  is not reached
- 6     **and** the maximum number of clusters  $\mathbf{K}$  is not reached **then**
- 7     | save the best refinement  $\{S_j\}_j$  and update the best score  $b$ .

---

**Remark 7** (Heuristic behind the choice of the active subspaces metric for K-medoids). Having in mind that the optimal profile  $h(y) = \mathbb{E}_{\mu_i}[f|P_{r(S_i),i}]$  from definition 1 is approximated as  $h(y) = f(y) = f(P_r \mathbf{x})$  as reported in remark 3, we can argue that clustering with the AS metric from equation (7) is effective since, for this choice of the metric, the clusters tend to form transversally with respect to the active subspace directions. This is because the metric weights more the components with higher eigenvalues. So clustering with this metric reduces heuristically also the approximation error induced by the choice of the non-optimal profile.

Other clustering criterions employed must satisfy the subspace Poincaré inequality for each cluster. Regarding the regression method we employ Gaussian process regression with RBF-ARD kernel [41]. The procedure for response surface design with Gaussian processes and ridge approximation with active subspaces can be found in [6, 27]. As for the indicator for refinement, the local  $R^2$  score in remark 4 is employed to measure the accuracy of the ridge approximation against a validation dataset and the estimator from the RHS of equation (12) is used to determine the dimension of the active subspace of each cluster.

Regarding the complexity of the algorithm, for each refinement, considering an intermediate cluster of  $K$  elements, the most expensive tasks are the active subspace evaluation  $O(Knp^2 + Kn^2p + n^3)$  (the first two costs refer to matrix multiplications, while the third for eigendecomposition), the clustering algorithm, for example K-medoids with AS distance  $O(K(K-m)^2)$ , and the Gaussian process regression  $O(K^3p^3)$ , where  $p$  is the dimension of the outputs and  $m$  is the minimum number of children clusters. With  $M$  we denote the maximum number of children clusters. At each refinement level, the most costly operation is the Gaussian process regression. In the worst case the height of the refinement tree is  $l = \log_m N/el$  where  $el$  is the minimum number of elements per cluster. From table 1, assuming  $p = 1$ , it can be noticed that at the beginning the most expensive operation is the clustering algorithm (especially when  $k \ll N$ , in general  $N > n$ ), while near the final refinement the most expensive operations are the GPR and the evaluation of the AS when  $m$  is moderately greater than the minimum number of elements  $el$  (in general it can happen to have  $m > el > r$ ). In fact, at the  $i$ -th refinement level the AS and GPR are computed  $(M-m)m^i$  times, while the clustering is performed  $m^i$  times.

## 4 Classification with local active subspace dimension

A poor design of the parameter space could add an avoidable complexity to the surrogate modelling algorithms. Often, in practical applications, each parameter range is chosen independently with respect to the others. Then, it is the responsibility of the surrogate modelling procedure to

Table 1: Computational complexity of hierarchical top-down clustering.

Step	Cost	Description
Root	$O(Nnp^2 + Nn^2p + n^3)$	AS
	$O(N^3p^3)$	GPR
First refinement:	$O(N(N-k)^2)$	K-medoids
$k$ from $m$ to $M$	$O((N/k)np^2 + (N/k)n^2p + n^3)$	AS
	$O((N/k)^3p^3)$	GPR
Intermediate refinements	-	-
Last refinement:	$O((N/k^{l-1})((N/k^{l-1}) - k)^2)$	K-medoids
$k$ from $m$ to $M$	$O((N/k^l)np^2 + (N/k^l)n^2p + n^3)$	AS
for each one of the $m^{l-1}$ clusters	$O((N/k^l)^3p^3)$	GPR

disentangle the correlations among the parameters. However, in this way, looking at the response surface from parameters to outputs, regions that present different degrees of correlation are treated indistinctly. In this matter, a good practice is to study as a preprocessing step some sensitivity measures, like the total Sobol indexes [35] among groups of parameters, and split the parameter space accordingly in order to avoid the use of more expensive surrogate modeling techniques later.

Of course Sobol indices or the global active subspace sensitivity scores give summary statistics on the whole domain. So in general, one could study the parameter space more in detail, classifying nonlinearly regions with respect to the complexity of the response surface, if there are enough samples to perform such studies.

We introduce an effective approach to tackle the problem of classification of the parameter space with respect to a local active subspace information. With the latter we mean two possible alternatives.

**Definition 2** (Local active subspace dimension). *Given a threshold  $\epsilon > 0$ , the pairs of inputs and gradients  $\{(\mathbf{X}_i, \mathbf{dY}_i)\}_i$  associated to an objective function of interest  $f : \mathcal{X} \subset \mathbb{R}^n \rightarrow \mathbb{R}$ , the size of the neighbour of sample points to consider  $N \geq n$ , and a subsampling parameter  $p \in \mathbb{N}$ ,  $p \leq N$ , the local active subspace dimension  $r_i$  associated to a sample point  $\mathbf{X}_i \in \mathcal{X}$  is the positive integer*

$$r_i = \operatorname{argmin}_{1 \leq r \leq p} \left\{ \operatorname{tr} \left( (Id - P_r) \left( \frac{1}{p} \sum_{i \in J} \mathbf{dY}_i \otimes \mathbf{dY}_i \right) (Id - P_r) \right) \leq \epsilon \mid J \in C(N, p) \right\}, \quad (24)$$

where  $C(N, p)$  is the set of combinations without repetition of the  $N$  elements of the Euclidean neighbour of  $\mathbf{X}_i$  with class  $p$ .

**Definition 3** (Local active subspace). *Given the pairs of inputs and gradients  $\{(\mathbf{X}_i, \mathbf{dY}_i)\}_i$  associated to an objective function of interest  $f : \mathcal{X} \subset \mathbb{R}^n \rightarrow \mathbb{R}$ , the size of the neighbour of sample points to consider  $N \geq n$ , and a fixed dimension  $p \in \mathbb{N}$ ,  $1 \leq p \leq N$ , the local active subspace  $W_i$  associated to a sample point  $\mathbf{X}_i \in \mathcal{X}$  is the matrix of the first  $p$  eigenvectors of the spectral decomposition of*

$$(Id - P_r) \left( \frac{1}{p} \sum_{i \in U} \mathbf{dY}_i \otimes \mathbf{dY}_i \right) (Id - P_r), \quad (25)$$

where  $U$  is the neighbour of sample points of  $\mathbf{X}_i$  with respect to the Euclidean distance. In practice we choose  $p$  close to the global active subspace dimension. The pairs  $\{(\mathbf{X}_i, W_i)\}_i$  can be thought as a discrete vector bundle of rank  $p$  and  $\{W_i\}_i$  can be thought as a subset of points of the Grassmannian  $Gr(N, p)$ .

Starting from the pairs of inputs-gradients  $\{(\mathbf{X}_i, \mathbf{dY}_i)\}_i$ , the procedure follows the following steps:

1. Each parameter sample is enriched with the additional feature corresponding to the local active subspace dimension from definition 2 or the local active subspace from definition 3, represented by the variable  $\mathbf{Z}$ .

2. Each sample  $\mathbf{X}_i$  is labelled with an integer  $l_i$  that will be used as classification label in the next step. To label the pairs  $\{(\mathbf{X}_i, \mathbf{Z}_i)\}_i$  we selected K-medoids with Grassmanian metric

$$d((X_i, Z_i), (X_j, Z_j)) = \|Z_i - Z_j\|_F, \quad (26)$$

where  $\|\cdot\|_F$  is the Frobenious distance, in case  $\mathbf{Z}_i$  represents the local active subspace or spectral clustering in case  $\mathbf{Z}_i$  is the local active subspace dimension. In the last case, the labels correspond to the connected components of the graph built on the nodes  $\{(\mathbf{X}_i, \mathbf{Z}_i)\}_i$  with adjacency list corresponding to the nearest nodes with respect to the distance

$$d((X_i, Z_i), (X_j, Z_j)) = \begin{cases} \infty, & Z_i \neq Z_j \\ \|X_i - X_j\|, & Z_i = Z_j \end{cases}, \quad (27)$$

where  $\|\cdot\|$  is the Euclidean metric in  $\mathbb{R}^n$ . The connected components are obtained from the eigenvectors associated to the eigenvalue 0 of the discrete Laplacian of the graph [23].

3. A classification method is applied to the inputs-labels pairs  $\{(\mathbf{X}_i, l_i)\}_i$ . Generally, for our relatively simple applications we apply a multilayer perceptron with 1000 hidden nodes and 2 layers.

**Remark 8** (Grassmann distance). In general regarding the definition 3, the dimension  $p$  could be varying among samples  $\mathbf{X}_i$  and one could use a more general distance with respect to the one from equation (26) that can have as arguments two vectorial subspaces of possibly different and arbitrary large dimensions.

**Remark 9** (Gradient-free active subspace). In general both the response surface design and the classification procedure above can be carried out from the pairs  $\{(\mathbf{X}_i, \mathbf{Y}_i)\}_i$  of inputs, outputs instead of the sets  $\{(\mathbf{X}_i, \mathbf{dY}_i)\}_i$  of inputs, gradients. In fact, the gradients  $\{\mathbf{dY}_i\}$  can be approximated in many different ways [6] from  $\{(\mathbf{X}_i, \mathbf{Y}_i)\}_i$ . In the numerical results in section 5 when the gradients are not available they are approximated with the gradients of the local one-dimensional polynomial regression built on top of the neighbouring samples.

---

**Algorithm 5:** Classification with local features from the active subspaces information.

---

**input** : inputs-gradients pairs  $\{(\mathbf{X}_i, \mathbf{dY}_i)\}_{i \in I}$  as training dataset with index set  $I$ ,  
local features based on AS information  $\{\mathbf{Z}_i\}_{i \in I}$ , see definition 2 and definition 3,  
labelling method based on the distance  $d$  from equation (26) or from equation (27),  
classification method that takes as input the inputs-labels pairs  $\{(\mathbf{X}_i, l_i)\}_{i \in I}$

**output:** predictor for new test inputs and classes of the training dataset.

- 1 **foreach**  $i \in I$  **do**
  - 2    $\lfloor$  evaluate the feature  $\mathbf{Z}_i$  from  $(\mathbf{X}_i, \mathbf{dY}_i)$  and the neighbouring points of  $\mathbf{X}_i$ .
  - 3 initialize the  $|I| \times |I|$  distance matrix  $M$  associated to the pairs  $\{(\mathbf{X}_i, \mathbf{Z}_i)\}_{i \in I}$ .
  - 4 **foreach**  $i \in I$  **do**
  - 5    $\lfloor$  **foreach**  $i \leq j \in I$  **do**
  - 6      $\lfloor$   $M(i, j) = d((\mathbf{X}_i, \mathbf{Z}_i), (\mathbf{X}_j, \mathbf{Z}_j))$
  - 7 use the labelling method with input  $M$ , to assign a label  $l_i$  for each pair  $(\mathbf{X}_i, \mathbf{Z}_i)$ .
  - 8 train the classification method with the inputs-labels training pairs  $\{(\mathbf{X}_i, l_i)\}_{i \in I}$ .
- 

## 5 Numerical results

In this section we are going to apply the proposed localized AS method to some datasets of increasing complexity. We compare the clustering techniques we presented in section 3, and we show how the active subspaces-based distance metric outperforms the Euclidean one for those functions which present a global lower intrinsic dimensionality. We remark that for hierarchical top-down clustering we can use both metrics, and we always show the best case for the specific dataset.

We start from a bidimensional example for which we can actually plot the clusters and the regressions, and compare the different techniques. Even if it is not a case for which one should use parameter space dimensionality reduction we think it could be very useful for the reader to understand also visually all the proposed techniques. For the higher dimensional examples we compare the accuracy of the methods in terms of  $R^2$  score and classification performance.

All the computations regarding AS are done with the open source Python package<sup>1</sup> called ATHENA [28], for the classification algorithms we use the scikit-learn package [5] and for the Gaussian process regression GPpy [13].

## 5.1 Some illustrative bidimensional examples

We start by presenting two bidimensional test cases in order to be able to present every aspect of the methodology together with illustrative plots. First we analyse a case where a global active subspace, even if present, does not provide a regression accurate enough along the active direction in section 5.1.1. Then we consider a radial symmetric function for which, by construction, an AS does not exist in section 5.1.2 and the use of K-means is instead preferable since we cannot exploit a privileged direction in the input domain.

### 5.1.1 Quartic function

Let us consider the following bidimensional quartic function:

$$f(\mathbf{x}) = x_1^4 - x_2^4, \quad \mathbf{x} = (x_1, x_2) \in [0, 1]^2. \quad (28)$$

In figure 1 we can see the contour plot of the function, the active subspace direction — translated for illustrative reasons — and the corresponding sufficient summary plot of the global active subspace, computed using 400 uniformly distributed samples. With sufficient summary plot we intend  $f(\mathbf{x})$  plotted against the input parameters projected onto the active subspace, that is  $W_1^T \mathbf{x}$ . It is clear how, in this case, a univariate regression does not produce any useful prediction capability.

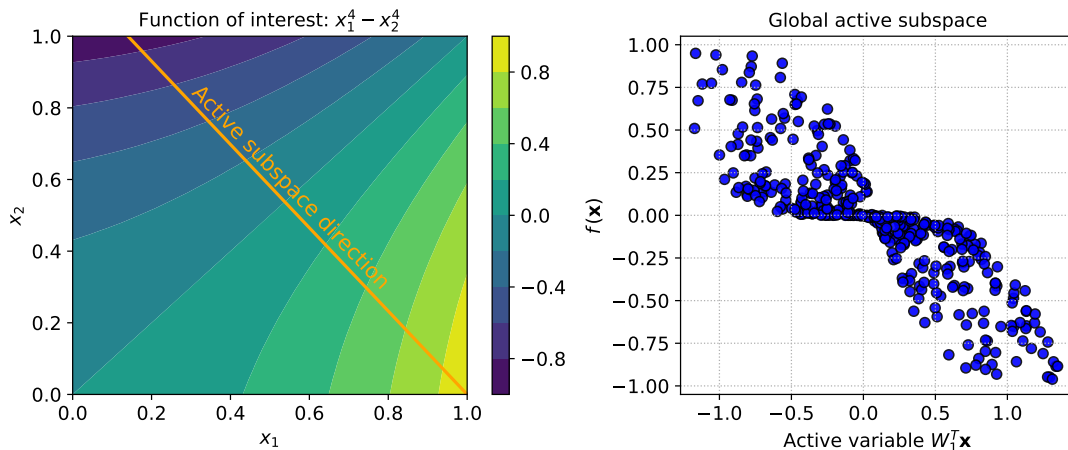


Figure 1: On the left panel the contour plot of the quartic function considered in equation (28) and in orange the global active subspace direction. On the right panel the sufficient summary plot resulting projecting the data onto the global AS.

Let us apply the clustering techniques introduced in the previous sections fixing the number of clusters to 4. In figure 2 we can clearly see how the supervised distance metric in equation (7) acts in dividing the input parameters. On the left panel we apply K-means which clusters the data into 4 uniform quadrants, while in the middle and right panels we have K-medoids and hierarchical top-down, respectively, with a subdivision aligned with the global AS. We notice that for this simple case the new metric induces an identical clustering of the data. In figure 3 we plotted the sufficient summary plots for each of the clusters individuated by K-medoids or hierarchical

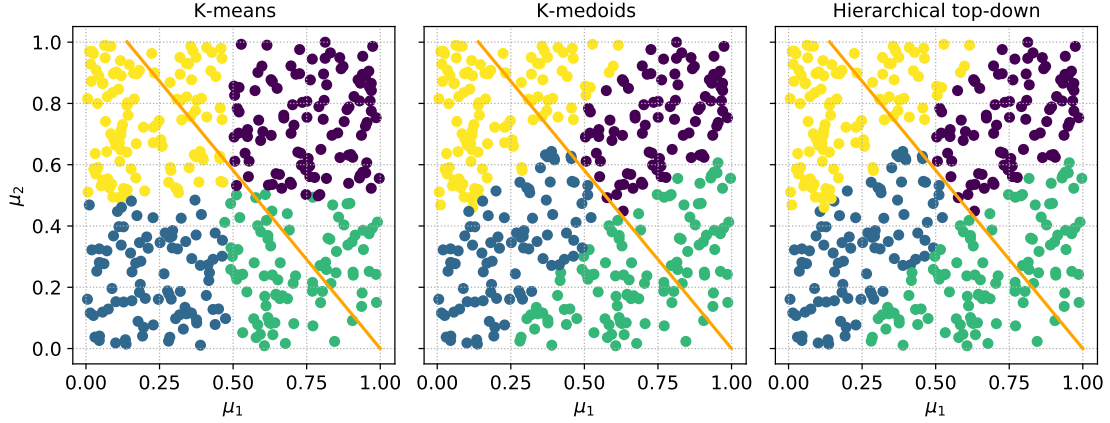


Figure 2: Comparison between the different clusters obtained by K-means (on the left), K-medoids (middle panel), and hierarchical top-down (on the right) with AS induced distance metric defined in equation (7) for the quartic test function. In orange the global active subspace direction. Every cluster is depicted in a different color.

top-down in figure 2. It is clear how by using a single univariate regression for each cluster the  $R^2$  score improves a lot with respect to a global approach (see right panel of figure 1).

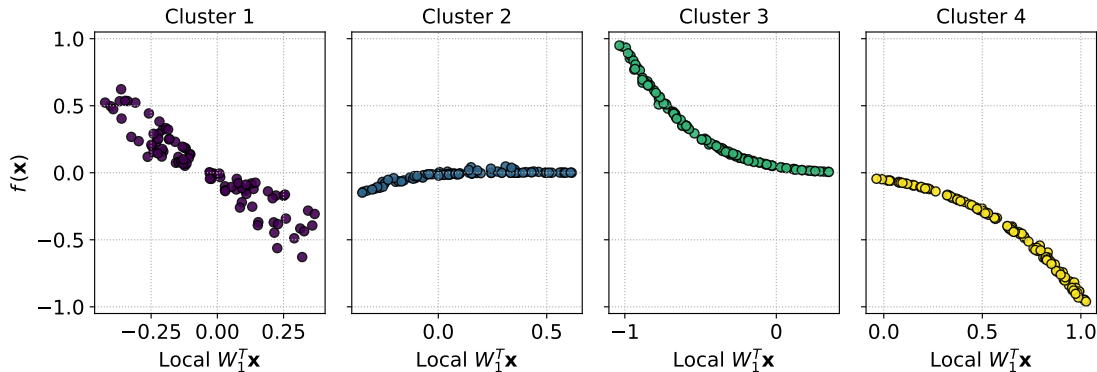


Figure 3: Local sufficient summary plots for the 4 clusters individuated by K-medoids or hierarchical top-down in figure 2 (colors correspond).

We can also compare the  $R^2$  scores for all the methods, using a test datasets of 600 samples. In figure 4 we report the scores for K-means, K-medoids and for hierarchical top-down with AS-based distance metric. The score for the global AS, which is 0.78, is not reported in figure 4 for illustrative reasons. The results are very similar due to the relatively simple test case, but we can see that even with 2 clusters the gain in accuracy is around 23% using the metric in equation (7).

The hierarchical top-down clustering method was ran with the following hyper-parameters: the total number of clusters is increasing from 2 to 10, the minimum number of children equal to the maximum number of children equal to 3, uniform normalization of the clusters, the minimum size of each cluster is 10 elements, the clustering method is K-medoids with AS distance, the maximum active subspace dimension is 1.

Then we want to increase the accuracy of the regression with 3 clusters, loosing in some regions the reduction in the parameter space. Starting from the clustering with hierarchical top-down and 3 clusters of dimension 1, the AS dimension of each of the 3 clusters is increased if the threshold of 0.95 on the local  $R^2$  score is not met. In general, the local  $R^2$  score is evaluated on a validation set, for which predictions from the local response surfaces are obtained, after each validation sample

<sup>1</sup>Available at <https://github.com/mathLab/ATHENA/>.

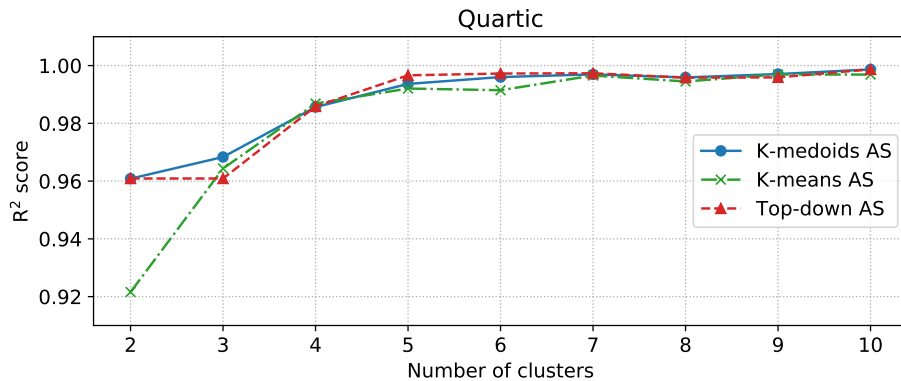


Figure 4:  $R^2$  scores comparison between local versions varying the number of clusters for the quartic function in equation (28). Global AS has a score equal to 0.78.

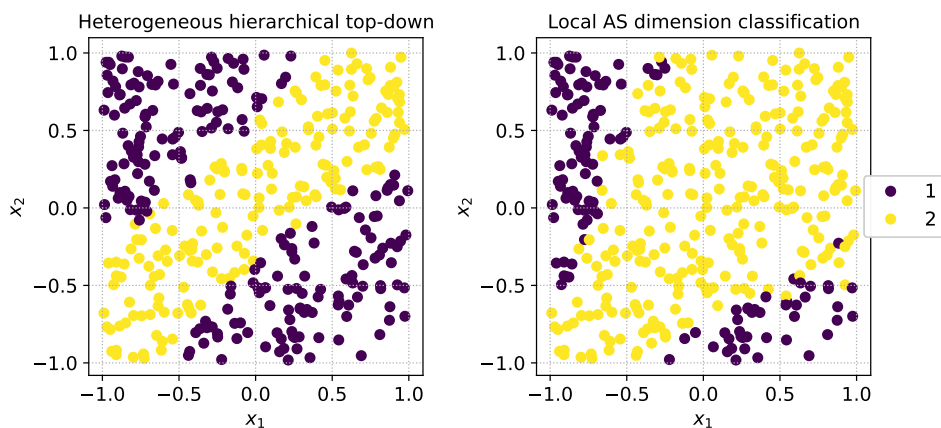


Figure 5: On the left panel the hierarchical top-down clustering with heterogeneous AS dimension and  $R^2$  score equal to 1. On the right panel the labels of the local AS dimension from definition 2.

is classified into one of the 3 clusters.

The 3 clusters are reported in figure 5 on the left. The  $R^2$  score on the test set is 1, instead of around 0.97 from figure 4. To obtain this result, the central cluster AS dimension is increased from 1 to 2. We compare the clustering with respect to the classification of the local AS dimension with algorithm 5 using as features the local AS dimension as defined in definition 2, on the right of figure 5. Actually algorithm 5 is stopped after the plotted labels are obtained as the connected components of the underlying graph to which spectral clustering is applied: no classification method is employed, yet. It can be seen that hierarchical top-down clustering with heterogeneous AS dimension is more efficient with respect to the classes of algorithm 5, regarding the number of samples associated to a response surface of dimension 2.

### 5.1.2 Radial symmetric cosine

This example addresses the case for which an active subspace is not present. This is due to the fact that there are no preferred directions in the input domain since the function  $f$  has a radial symmetry. For this case the exploitation of the supervised distance metric does not provide any significant gain and K-means clustering works better on average, since it does not use the global AS structure. The model function we consider is the following

$$f(\mathbf{x}) = \cos(\|\mathbf{x}\|^2), \quad \mathbf{x} \in [-3, 3]^2. \quad (29)$$

In figure 6 we compare the  $R^2$  scores for K-means, K-medoids with AS-based metric, and hierarchical top-down with Euclidean metric. We used 500 training samples and 500 test samples.

We see K-medoids has not a clear behaviour with respect to the number of clusters, while the other methods present a monotonic trend and better results on average, especially K-means. On the other hand local models improve the accuracy considerably, even for a small number of clusters, with respect to a global model.

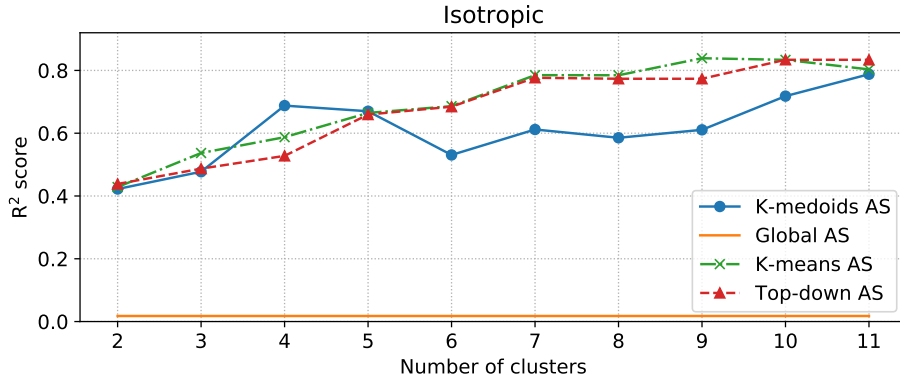


Figure 6:  $R^2$  scores comparison between global AS and local versions varying the number of clusters for the isotropic model function in equation (29). Global AS corresponds to no clustering.

In this case the specifics of hierarchical top-down clustering are: the minimum number of children is equal to the maximum, the minimum number of elements per cluster is 10, the clustering method chosen is K-means, the normalization employed is the uniform one, and the total number of clusters is increasing from 2 to 11.

## 5.2 High-dimensional datasets

In this section we consider some more interesting benchmarks, for which dimension reduction in the parameter space is more useful since the starting dimension of the parameter space is higher. We test the classification procedure in algorithm 5 with an objective function with 6 parameters and defined piecewise as a paraboloid with different AS dimensions. We also test the procedure of response surface design with local AS, with a classical 8-dimensional epidemic benchmark model.

### 5.2.1 Multi-dimensional hyper-paraboloid

The objective function  $f : [-4, 4]^6 \rightarrow \mathbb{R}$  we consider is defined piecewise as follows

$$f(x) = \begin{cases} x_1^2 & \text{if } x_1 > 0 \text{ and } x_2 > 0, \\ x_1^2 + x_2^2 & \text{if } x_1 < 0 \text{ and } x_2 > 0, \\ x_1^2 + x_2^2 + x_3^2 & \text{if } x_1 > 0 \text{ and } x_2 < 0, \\ x_1^2 + x_2^2 + x_3^2 + x_4^2 & \text{if } x_1 < 0 \text{ and } x_2 < 0. \end{cases} \quad (30)$$

In the 4 domains in which  $f$  is defined differently, we expect an AS dimension ranging from 1 to 4, respectively. We employed algorithm 5 using the local AS dimensions as additional features, from definition 2: the values of the hyper-parameters are the following:  $\epsilon = 0.999$ ,  $N = 6$ ,  $p = 4$ . In figure 7 we plot the accuracy of the classification of the labels, associated to the connected components of the graph built as described in algorithm 5, and also the accuracy of the classification of the local active subspace dimension, that takes the values from 1 to 4. The test dataset for both the classification errors has size 1000. The score chosen to assess the quality of the classification is the mean accuracy, that is the number of correctly predicted labels over the total number of labels. For both the classification tasks 100 train samples are enough to achieve a mean accuracy above 80%.

We remark that every step is applied to a dataset of samples in a parameter space of dimension 6, even if, to get a qualitative idea of the performances of the method, in figure 8 we show only the

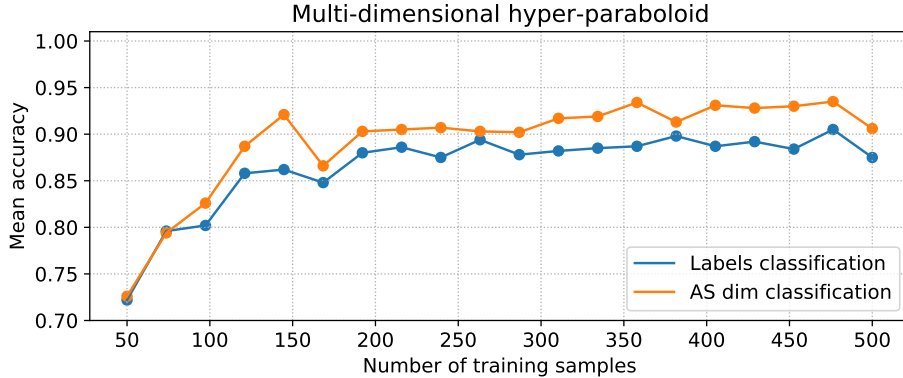


Figure 7: Mean accuracy study for a training dataset increasing in size from 50 to 500 samples. The test set is made of 1000 independent samples. The classification accuracy for the procedures of connected component classification (in blue) and local AS dimension classification (in orange) are both shown.

first two components of the decision boundaries of the 4 classes for both the previously described classification problems.

### 5.2.2 Ebola epidemic model

In this section we examine the performance of the proposed methods over the dataset created with the SEIR model for the spread of Ebola<sup>2</sup>. The output of interest in this case is the basic reproduction number  $R_0$  of the SEIR model, described in [11], which is computed using 8 parameters as follows

$$R_0 = \frac{\beta_1 + \frac{\beta_2 \rho_1 \gamma_1}{\omega} + \frac{\beta_3}{\gamma_2} \psi}{\gamma_1 + \psi}. \quad (31)$$

As shown in previous works, this function has a lower intrinsic dimensionality, and thus a meaningful active subspace, in particular of dimension 1. To evaluate the performance of the local AS we compute the  $R^2$  score, as in equation (15), varying the number of clusters from 2 to 10 for all the methods presented. The test and training datasets are composed by 500 and 300, respectively, uniformly distributed and independent samples. The results are reported in figure 9, where as baseline we reported the  $R^2$  for the GPR over the global AS. We can see how the use of the AS-based distance metric contributes the most with respect to the actual clustering method (compare K-medoids and hierarchical top-down in the plot). K-means, instead, does not guarantee an improved accuracy (for 4 and 9 clusters), and in general the gain is limited with respect to the other methods, especially for a small number of clusters which is the most common case in practice, since usually we work in a data scarcity regime. The results for K-medoids and top-down are remarkable even for a small amount of clusters with an  $R^2$  above 0.9 and an improvement over 10% with respect to the global AS, which means that no clustering have been used.

The hyper-parameters for the hierarchical top-down algorithm are the following: the maximum local active subspace dimension is 1, the maximum number of children is equal to the number of total clusters, the minimum number of children is 2 at each refinement level, the minimum number of elements per cluster is 10, and the clustering method for each refinement is K-medoids with AS distance.

### 5.3 Datasets with vectorial outputs

In this section we want to show how hierarchical top-down clustering and the classification procedure of algorithm 5 can be combined to improve the overall reduction in the parameter space, for a fixed lower threshold in the  $R^2$  score. For the response surface design with active subspaces for vectorial outputs we refer to [43, 27].

<sup>2</sup>The dataset was taken from <https://github.com/paulcon/as-data-sets>.

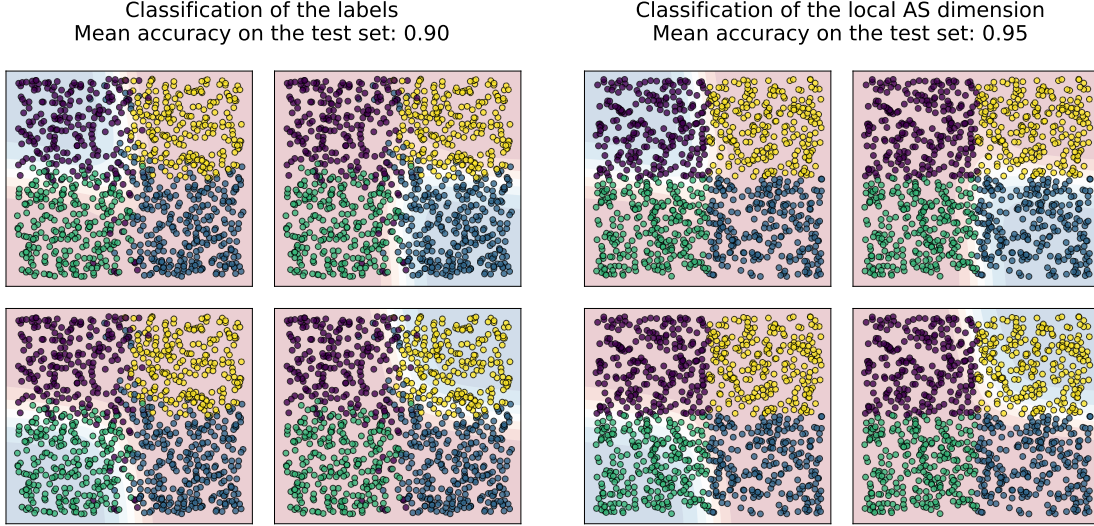


Figure 8: On the left panel the decision boundaries of the 4 classes associated to the connected components of the graph built as described in algorithm 5. On the right panel the decision boundaries of the 4 classes associated to the local AS dimension from 1 to 4. The datasets has dimension 6, only the first two components of the decision boundaries and of the test samples are plotted.

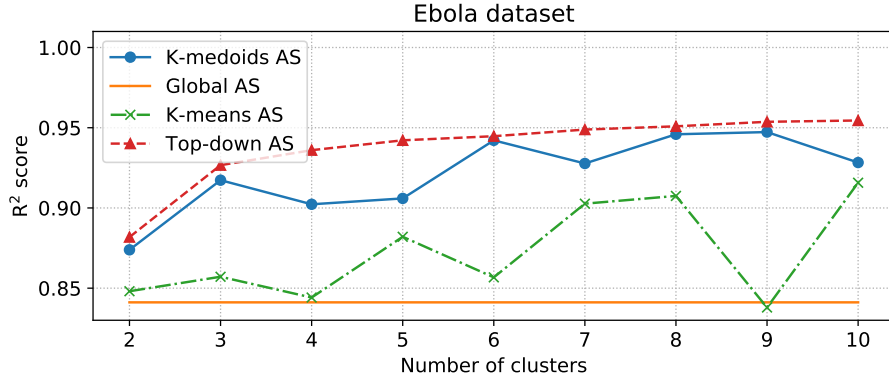


Figure 9:  $R^2$  scores comparison between global AS and local versions varying the number of clusters for the Ebola spread model defined in equation (31). Global AS corresponds to no clustering.

### 5.3.1 Poisson equation with random diffusivity

Let us consider the stochastic Poisson problem on the square  $\mathbf{x} = (x, y) \in \Omega := [0, 1]^2$ , defined as:

$$\begin{cases} -\nabla \cdot (\kappa \nabla u) = 1, & \mathbf{x} \in \Omega, \\ u = 0, & \mathbf{x} \in \partial\Omega_{\text{top}} \cup \partial\Omega_{\text{bottom}}, \\ u = 10y(1 - y), & \mathbf{x} \in \partial\Omega_{\text{left}}, \\ \mathbf{n} \cdot \nabla u = 0, & \mathbf{x} \in \partial\Omega_{\text{right}}, \end{cases} \quad (32)$$

with homogeneous Neumann boundary condition on  $\partial\Omega_{\text{right}}$ , and Dirichlet boundary conditions on the remaining part of  $\partial\Omega$ . The diffusion coefficient  $\kappa : (\Omega, \mathcal{A}, P) \times \Omega \rightarrow \mathbb{R}$ , with  $\mathcal{A}$  denoting a  $\sigma$ -algebra, is such that  $\log(\kappa)$  is a Gaussian random field, with covariance function  $G(\mathbf{x}, \mathbf{y})$  defined by

$$G(\mathbf{x}, \mathbf{y}) = \exp\left(-\frac{\|\mathbf{x} - \mathbf{y}\|^2}{\beta^2}\right), \quad \forall \mathbf{x}, \mathbf{y} \in \Omega, \quad (33)$$

where the correlation length is  $\beta = 0.03$ . We approximate this random field with the truncated Karhunen–Loève decomposition as

$$\kappa(s, \mathbf{x}) \approx \exp \left( \sum_{i=0}^m X_i(s) \gamma_i \psi_i(\mathbf{x}) \right), \quad \forall (s, \mathbf{x}) \in \Omega \times \Omega, \quad (34)$$

where  $(X_i)_{i \in 1, \dots, m}$  are independent standard normal distributed random variables, and the eigenpairs of the Karhunen–Loève decomposition of the zero-mean random field  $\kappa$  are denoted with  $(\gamma_i, \psi_i)_{i \in 1, \dots, d}$ . The parameters  $(X_i)_{i \in 1, \dots, m=10}$  sampled from a standard normal distribution are the coefficients of the Karhunen–Loève expansion, truncated at the first 10 modes, so the parameter space has dimension  $m = 10$ .

The domain  $\Omega$  is discretized with a triangular unstructured mesh  $\mathcal{T}$  with 3194 triangles. The simulations are carried out with the finite element method with polynomial order 1. The solution  $u$  is evaluated at 1668 degrees of freedom, thus the output is vectorial with dimension  $d = 1688$ . As done in [43, 27], the output is enriched with the metric induced by the Sobolev space  $H^1(\Omega)$  on to the finite element space of polynomial order 1: the metric is thus represented by a  $d \times d$  matrix  $M$  obtained as the sum of the mass and stiffness matrices of the numerical scheme and it is involved in the AS procedure when computing the correlation matrix  $\mathbb{E} [Df M Df^T]$ , where  $Df$  is the  $m \times d$  Jacobian matrix of the objective function  $f : \mathbb{R}^{10} \rightarrow \mathbb{R}^d$ .

Since the output is high-dimensional we classified with algorithm 5 the output space in 6 clusters, using the Grassmann distance from equation (26), as shown in figure 10.

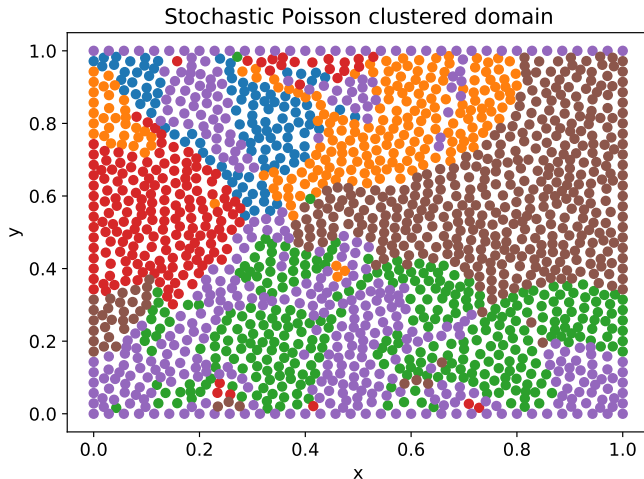


Figure 10: Subdivision of the spatial domain  $\Omega$  in 6 clusters based on the Grassmann distance from definition 3, i.e. the clusters correspond to the connected components of the graph built on top of the degrees of freedom with adjacency list determined using as distance definition 3.

Afterwards we applied hierarchical top-down clustering to every one of the 6 triples of inputs-outputs-gradients, obtained restricting the outputs and the gradients to each one of the 6 clusters. The specifics of hierarchical top-down clustering we employed are the following: the minimum and maximum number of children for each refinement are equal to the total number of clusters, which is 4, the minimum number of elements in each cluster is 10, and the clustering algorithm chosen is K-medoids with the AS distance. The size of the training and test datasets is respectively of 500 and 150. The gradients are evaluated with the adjoint method. Since the output is vectorial we employed the mean  $R^2$  score, where the average is made among the components of the vectorial output considered.

Then for every lower threshold on the  $R^2$  score we increase one by one the dimension of the  $6 \times 4$  local clusters, until all the  $R^2$  scores of each of the 6 triples are above the fixed threshold. The same procedure is applied to the whole dataset of inputs-outputs-gradients but executing hierarchical top-down clustering just once, for all the output’s components altogether.

The results are reported in figure 11. In the case of the clustered outputs, the local dimension of each one of the 6 clustered outputs times 4 local clusters in the parameter space, for a total

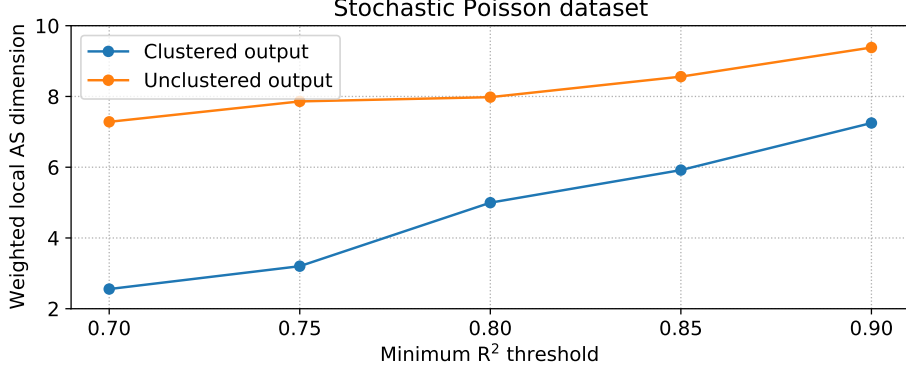


Figure 11: In orange the local AS dimensions weighted on the number of elements of each of the 4 clusters in the parameter space, obtained with hierarchical top-down clustering. In blue the local AS dimensions weighted on the number of elements of each of the 4 clusters in the parameter space, obtained with hierarchical top-down clustering, times 6 clustered outputs (see figure 10) for a total of 24 terms in the weighted average.

of 24 local clusters, are weighted with the number of elements of each cluster. In the same way the 4 clusters of the case with unclustered outputs is weighted with the number of the elements of each one of the 4 clusters. It can be seen that for every fixed threshold, there is an evident gain, with respect to the dimension reduction in the parameter space, in clustering the outputs and then performing hierarchical top-down clustering in the parameter space.

### 5.3.2 Shape design of an airfoil

For this vectorial test case we consider the temporal evolution of the lift coefficient of a parametrized NACA airfoil. Here we briefly present the problem we solve to create the dataset, we refer to [38] for a deeper description.

Let us consider the unsteady incompressible Navier-Stokes equations described in an Eulerian framework on a parametrized space-time domain  $S(\boldsymbol{\mu}) = \Omega(\boldsymbol{\mu}) \times [0, T] \subset \mathbb{R}^2 \times \mathbb{R}^+$ . The vectorial velocity field  $\mathbf{u} : S(\boldsymbol{\mu}) \rightarrow \mathbb{R}^2$ , and the scalar pressure field  $p : S(\boldsymbol{\mu}) \rightarrow \mathbb{R}$  solve the following parametric PDE:

$$\begin{cases} \mathbf{u}_t + \nabla \cdot (\mathbf{u} \otimes \mathbf{u}) - \nabla \cdot 2\nu \nabla^s \mathbf{u} = -\nabla p & \text{in } S(\boldsymbol{\mu}), \\ \nabla \cdot \mathbf{u} = 0 & \text{in } S(\boldsymbol{\mu}), \\ \mathbf{u}(t, x) = \mathbf{f}(\mathbf{x}) & \text{on } \Gamma_{\text{in}} \times [0, T], \\ \mathbf{u}(t, x) = 0 & \text{on } \Gamma_0(\boldsymbol{\mu}) \times [0, T], \\ (\nu \nabla \mathbf{u} - p \mathbf{I}) \mathbf{n} = 0 & \text{on } \Gamma_{\text{out}} \times [0, T], \\ \mathbf{u}(0, \mathbf{x}) = \mathbf{k}(\mathbf{x}) & \text{in } S(\boldsymbol{\mu})_0 \end{cases} \quad (35)$$

Here,  $\Gamma = \Gamma_{\text{in}} \cup \Gamma_{\text{out}} \cup \Gamma_0$  denotes the boundary of  $\Omega(\boldsymbol{\mu})$  composed by inlet boundary, outlet boundary, and physical walls, respectively. With  $\mathbf{f}(\mathbf{x})$  we indicate the stationary non-homogeneous boundary condition, and with  $\mathbf{k}(\mathbf{x})$  the initial condition for the velocity at  $t = 0$ . The geometrical deformation are applied to the boundary  $\Gamma_0(\boldsymbol{\mu})$ . The undeformed configuration corresponds to the NACA 4412 wing profile [1, 17]. To alter such geometry, we adopt the shape parametrization and morphing technique proposed in [16], where 5 shape functions are added to the airfoil profiles. Let  $y_u$  and  $y_l$  be the upper and lower ordinates of the profile, respectively. The deformation of such coordinates is described as follows

$$y_u = \bar{y}_u + \sum_{i=1}^5 c_i r_i, \quad y_l = \bar{y}_l - \sum_{i=1}^5 d_i r_i, \quad (36)$$

where the bar denotes the reference undeformed state. The parameters  $\boldsymbol{\mu} \in \mathbb{D} \subset \mathbb{R}^{10}$  are the weights coefficients,  $c_i$  and  $d_i$ , associated with the shape functions  $r_i$ . In particular we set  $\mathbb{D} := [0, 0.03]^{10}$ . The explicit formulation of the shape functions can be found in [16]. For this datasets, the Reynolds

number is  $Re = 50000$ . The time step is  $dt = 1e - 3s$ . For other specifics regarding the solver employed and the numerical method adopted see [38].

As outputs we considered the values of the lift coefficient, every 15 time steps from  $100ms$  to  $30000ms$ , for a total of 1994 components. Even in this case the output is classified with algorithm 5 with distance defined in definition 2. The values of the lift coefficient physically interesting are collected at last, after an initialization phase. Nonetheless for the purpose of having a vectorial output we considered its value from the time instant  $100ms$ . The procedure finds two classes and splits the ordered output components in two parts: from the component 0 to 996, the local AS dimension is 1, for the remaining time steps it is higher. So we can expect an improvement on the efficiency of the reduction in the parameter space when considering separately these two sets of outputs components as figure 12 shows. The weighted local AS dimension is in fact lower when using clustering, for every minimum  $R^2$  threshold.

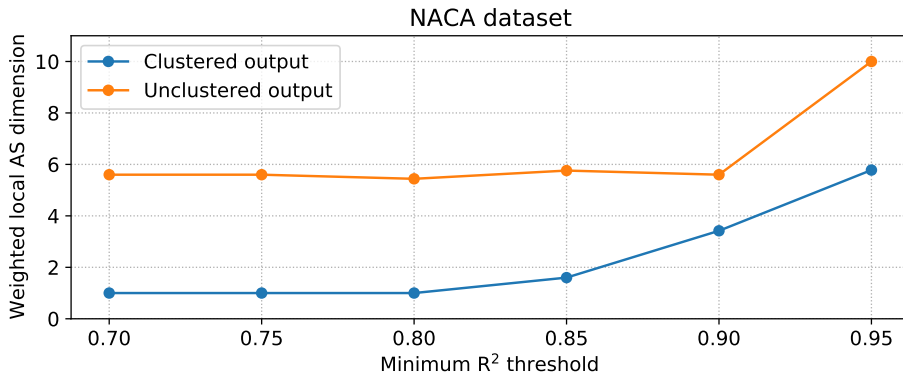


Figure 12: In orange the local AS dimensions weighted on the number of elements of each of the 2 clusters in the parameter space, obtained with hierarchical top-down clustering. In blue the local AS dimensions weighted on the number of elements of each of the 2 clusters in the parameter space, obtained with hierarchical top-down clustering, times 2 clustered outputs for a total of 4 terms in the weighted average.

## 6 Conclusions and perspectives

In this work we present a new local approach for parameter space reduction which exploits supervised clustering techniques, such as K-means, K-medoids, and hierarchical top-down, with a distance metric based on active subspaces. We called this method local active subspaces (LAS).

The theoretical formulation provides error estimates for the construction of response surfaces over the local active subspaces. We also present a classification approach to capture the optimal AS dimension for each cluster and can be used as a preprocessing step, both for the inputs and the vectorial outputs, for the construction of more accurate regressions and surrogate modeling. The proposed approach is very versatile, especially the hierarchical top-down clustering which can incorporate quite different criteria. The methodology has been validated over a vast range of datasets, both scalar and vector-valued, showing all the strengths and a possible weakness, in case of radial symmetric functions. In all the test cases LAS achieved superior performance with respect to the classical global approach.

Possible future lines of research can focus on the study of the extension of this methods to nonlinear parameter space reduction techniques, or on the use of more advanced clustering criteria.

## A Appendix

*Proof.* Let us use the notation  $h_1(x_1) := x_1(x_1 + \epsilon)(x_1 - \epsilon)$ , and  $h_2(x_2) := \cos(\omega x_2)$ , it can be shown that

$$\begin{aligned}\mathbb{E}_\mu [\nabla f \otimes \nabla f] &= \int_B \begin{pmatrix} (h_1')^2 (h_2)^2 & h_1 h_1' h_2 h_2' \\ h_1 h_1' h_2 h_2' & (h_1)^2 (h_2')^2 \end{pmatrix} d\mu(\mathbf{x}) + \mu(A \cup C) \cdot \begin{pmatrix} 1 & 0 \\ 0 & 0 \end{pmatrix} \\ &= \begin{pmatrix} \frac{2}{5}\epsilon^5 \left(1 + \frac{\sin(2\omega)}{2\omega}\right) & 0 \\ 0 & \frac{4}{105}\omega^2 \epsilon^7 \left(1 - \frac{\cos(2\omega)}{2\omega}\right) \end{pmatrix} + \mu(A \cup C) \cdot \begin{pmatrix} 1 & 0 \\ 0 & 0 \end{pmatrix},\end{aligned}$$

thus, since we are considering a one dimensional active subspace, the active eigenvector belongs to the set  $\{(1, 0), (0, 1)\}$ . Similarly we evaluate

$$\begin{aligned}\mathbb{E}_{\mu_B} [\nabla f|_B \otimes \nabla f|_B] &= \begin{pmatrix} \frac{8}{5}\epsilon^4 \left(1 + \frac{\sin(2\omega)}{2\omega}\right) & 0 \\ 0 & \frac{16}{105}\omega^2 \epsilon^6 \left(1 - \frac{\cos(2\omega)}{2\omega}\right) \end{pmatrix}, \\ \mathbb{E}_{\mu_A} [\nabla f|_A \otimes \nabla f|_A] &= \mathbb{E}_{\mu_C} [\nabla f|_C \otimes \nabla f|_C] = \begin{pmatrix} 1 & 0 \\ 0 & 0 \end{pmatrix},\end{aligned}$$

and conclude that there exist  $\epsilon > 0, \omega > 0$  such that:

$$\frac{2}{5}\epsilon^5 \left(1 + \frac{\sin(2\omega)}{2\omega}\right) + 4(1 - \epsilon) \geq \frac{4}{105}\omega^2 \epsilon^7 \left(1 - \frac{\cos(2\omega)}{2\omega}\right), \quad (1)$$

$$\frac{8}{5}\epsilon^4 \left(1 + \frac{\sin(2\omega)}{2\omega}\right) \leq \frac{16}{105}\omega^2 \epsilon^6 \left(1 - \frac{\cos(2\omega)}{2\omega}\right), \quad (2)$$

for example  $\epsilon \sim 10^{-2}, \omega \sim 10^4$  (approximately  $10\epsilon^{-2} \leq \omega^2 \leq 10\epsilon^{-7}$ ). In this way, using the notations of definition 1, we have

$$P_{1,\mathcal{X}} = e_1 \otimes e_1, \quad P_{1,A} = P_{1,C} = e_1 \otimes e_1, \quad P_{1,B} = e_2 \otimes e_2,$$

and it follows that

$$\mathbb{E}_\mu [\|f - R_{AS}(r, f)\|^2] = \mathbb{E}_\mu [f^2|_B] = (1/\mu(\mathcal{X})) \|h_1\|_{L^2(\mathcal{X},\lambda)}^2 \|h_2\|_{L^2(\mathcal{X},\lambda)}^2,$$

$$\begin{aligned}\mathbb{E}_\mu [\|f - \mathbb{E}_\mu [f|P_r] \circ P_r\|^2] &= (1/\mu(\mathcal{X})) \|h_1\|_{L^2(\mathcal{X},\lambda)}^2 \|h_2 - (1/\mu(\mathcal{X})) \int h_2 dx_2\|_{L^2(\mathcal{X},\lambda)}^2 \\ &= (1/\mu(\mathcal{X})) \|h_1\|_{L^2(\mathcal{X},\lambda)}^2 \left( \|h_2\|_{L^2(\mathcal{X},\lambda)}^2 - \frac{7}{16} \left( \int h_2 dx_2 \right)^2 \right),\end{aligned}$$

where  $\lambda$  is the Lebesgue measure. □

## Acknowledgements

This work was partially supported by an industrial Ph.D. grant sponsored by Fincantieri S.p.A. (IRONTH Project), by MIUR (Italian ministry for university and research) through FARE-X-AROMA-CFD project, and partially funded by European Union Funding for Research and Innovation — Horizon 2020 Program — in the framework of European Research Council Executive Agency: H2020 ERC CoG 2015 AROMA-CFD project 681447 “Advanced Reduced Order Methods with Applications in Computational Fluid Dynamics” P.I. Professor Gianluigi Rozza.

## References

- [1] I. H. Abbott and A. E. Von Doenhoff. *Theory of wing sections: including a summary of airfoil data*. Courier Corporation, 2012.
- [2] D. Amsallem and C. Farhat. Interpolation method for adapting reduced-order models and application to aeroelasticity. *AIAA journal*, 46(7):1803–1813, 2008.

- [3] K. Basu and A. B. Owen. Transformations and Hardy–Krause Variation. *SIAM Journal on Numerical Analysis*, 54(3):1946–1966, 2016.
- [4] R. A. Bridges, A. D. Gruber, C. R. Felder, M. Verma, and C. Hoff. Active Manifolds: A non-linear analogue to Active Subspaces. In *Proceedings of the 36th International Conference on Machine Learning, ICML 2019*, pages 764–772, Long Beach, California, USA, 9–15 June 2019.
- [5] L. Buitinck, G. Louppe, M. Blondel, F. Pedregosa, A. Mueller, O. Grisel, V. Niculae, P. Prettenhofer, A. Gramfort, J. Grobler, R. Layton, J. VanderPlas, A. Joly, B. Holt, and G. Varoquaux. API design for machine learning software: experiences from the scikit-learn project. In *ECML PKDD Workshop: Languages for Data Mining and Machine Learning*, pages 108–122, 2013.
- [6] P. G. Constantine. *Active subspaces: Emerging ideas for dimension reduction in parameter studies*, volume 2 of *SIAM Spotlights*. SIAM, 2015.
- [7] T. Daniel, F. Casenave, N. Akkari, and D. Ryckelynck. Model order reduction assisted by deep neural networks (ROM-net). *Advanced Modeling and Simulation in Engineering Sciences*, 7(1):1–27, 2020.
- [8] N. Demo, M. Tezzele, A. Mola, and G. Rozza. Hull shape design optimization with parameter space and model reductions, and self-learning mesh morphing. *Journal of Marine Science and Engineering*, 9(2):185, 2021.
- [9] N. Demo, M. Tezzele, and G. Rozza. A non-intrusive approach for reconstruction of POD modal coefficients through active subspaces. *Comptes Rendus Mécanique de l’Académie des Sciences, DataBEST 2019 Special Issue*, 347(11):873–881, November 2019.
- [10] N. Demo, M. Tezzele, and G. Rozza. A supervised learning approach involving active subspaces for an efficient genetic algorithm in high-dimensional optimization problems. *SIAM Journal on Scientific Computing*, 43(3):B831–B853, 2021.
- [11] P. Diaz, P. Constantine, K. Kalmbach, E. Jones, and S. Pankavich. A modified SEIR model for the spread of Ebola in Western Africa and metrics for resource allocation. *Applied Mathematics and Computation*, 324:141–155, 2018.
- [12] G. H. Golub and C. F. Van Loan. *Matrix computations*, volume 3. Johns Hopkins University Press, 2013.
- [13] GPy. GPy: A Gaussian process framework in Python. <http://github.com/SheffieldML/GPy>, since 2012.
- [14] J. Han, M. Kamber, and J. Pei. Data Mining: Concepts and Techniques. *The Morgan Kaufmann Series in Data Management Systems*, 5(4):83–124, 2012.
- [15] T. Hastie and R. Tibshirani. Discriminant adaptive nearest neighbor classification. *IEEE transactions on pattern analysis and machine intelligence*, 18(6):607–616, 1996.
- [16] R. M. Hicks and P. A. Henne. Wing Design by Numerical Optimization. *Journal of Aircraft*, 15(7):407–412, 1978.
- [17] E. N. Jacobs, K. E. Ward, and R. M. Pinkerton. The Characteristics of 78 Related Airfoil Sections from Tests in the Variable-Density Wind Tunnel. Technical Report 430, N.A.C.A., 1933.
- [18] L. Kaufman and P. J. Rousseeuw. *Finding Groups in Data: An Introduction to Cluster Analysis*, volume 344 of *Wiley Series in Probability and Statistics*. John Wiley & Sons, 2005.
- [19] K.-C. Li. Sliced inverse regression for dimension reduction. *Journal of the American Statistical Association*, 86(414):316–327, 1991.
- [20] A. E. Løvgrén, Y. Maday, and E. M. Rønquist. A reduced basis element method for the steady Stokes problem. *ESAIM: Mathematical Modelling and Numerical Analysis*, 40(3):529–552, 2006.

- [21] T. W. Lukaczyk, P. Constantine, F. Palacios, and J. J. Alonso. Active subspaces for shape optimization. In *10th AIAA multidisciplinary design optimization conference*, page 1171, 2014.
- [22] F. E. Maranzana. On the Location of Supply Points to Minimize Transport Costs. *Journal of the Operational Research Society*, 15(3):261–270, 1964.
- [23] K. P. Murphy. *Machine learning: a probabilistic perspective*. MIT press, 2012.
- [24] M. T. Parente, J. Wallin, B. Wohlmuth, et al. Generalized bounds for active subspaces. *Electronic Journal of Statistics*, 14(1):917–943, 2020.
- [25] H.-S. Park and C.-H. Jun. A simple and fast algorithm for K-medoids clustering. *Expert Systems with Applications*, 36(2):3336–3341, 2009.
- [26] A. Pinkus. *Ridge functions*, volume 205. Cambridge University Press, 2015.
- [27] F. Romor, M. Tezzele, A. Lario, and G. Rozza. Kernel-based Active Subspaces with application to CFD parametric problems using Discontinuous Galerkin method. *arXiv preprint arXiv:2008.12083*, 2020.
- [28] F. Romor, M. Tezzele, and G. Rozza. ATHENA: Advanced Techniques for High dimensional parameter spaces to Enhance Numerical Analysis. *arXiv preprint arXiv:2105.06713*, 2020.
- [29] F. Romor, M. Tezzele, and G. Rozza. Multi-fidelity data fusion for the approximation of scalar functions with low intrinsic dimensionality through active subspaces. In *Proceedings in Applied Mathematics & Mechanics*, volume 20. Wiley Online Library, 2021.
- [30] G. Rozza, M. Hess, G. Stabile, M. Tezzele, and F. Ballarin. Basic Ideas and Tools for Projection-Based Model Reduction of Parametric Partial Differential Equations. In P. Benner, S. Grivet-Talocia, A. Quarteroni, G. Rozza, W. H. A. Schilders, and L. M. Silveira, editors, *Model Order Reduction*, volume 2, chapter 1, pages 1–47. De Gruyter, Berlin, Boston, 2020.
- [31] G. Rozza, M. H. Malik, N. Demo, M. Tezzele, M. Girfoglio, G. Stabile, and A. Mola. Advances in Reduced Order Methods for Parametric Industrial Problems in Computational Fluid Dynamics. In R. Owen, R. de Borst, J. Reese, and P. Chris, editors, *ECCOMAS ECFD 7 - Proceedings of 6th European Conference on Computational Mechanics (ECCM 6) and 7th European Conference on Computational Fluid Dynamics (ECFD 7)*, pages 59–76, Glasgow, UK, 2018.
- [32] F. Salmoiraghi, F. Ballarin, G. Corsi, A. Mola, M. Tezzele, and G. Rozza. Advances in geometrical parametrization and reduced order models and methods for computational fluid dynamics problems in applied sciences and engineering: Overview and perspectives. *ECCOMAS Congress 2016 - Proceedings of the 7th European Congress on Computational Methods in Applied Sciences and Engineering*, 1:1013–1031, 2016.
- [33] E. Schubert and P. J. Rousseeuw. Faster k-medoids clustering: improving the PAM, CLARA, and CLARANS algorithms. In *International conference on similarity search and applications*, pages 171–187. Springer, 2019.
- [34] M. Sugiyama. Dimensionality reduction of multimodal labeled data by local Fisher discriminant analysis. *Journal of machine learning research*, 8(5), 2007.
- [35] T. J. Sullivan. *Introduction to Uncertainty Quantification*, volume 63. Springer, 2015.
- [36] M. Tezzele, F. Ballarin, and G. Rozza. Combined parameter and model reduction of cardiovascular problems by means of active subspaces and POD-Galerkin methods. In D. Boffi, L. F. Pavarino, G. Rozza, S. Scacchi, and C. Vergara, editors, *Mathematical and Numerical Modeling of the Cardiovascular System and Applications*, volume 16 of *SEMA-SIMAI Series*, pages 185–207. Springer International Publishing, 2018.
- [37] M. Tezzele, N. Demo, A. Mola, and G. Rozza. An integrated data-driven computational pipeline with model order reduction for industrial and applied mathematics. *Special Volume ECMI, In Press*, 2020.

- [38] M. Tezzele, N. Demo, G. Stabile, A. Mola, and G. Rozza. Enhancing CFD predictions in shape design problems by model and parameter space reduction. *Advanced Modeling and Simulation in Engineering Sciences*, 7(40), 2020.
- [39] M. Tezzele, F. Salmoiraghi, A. Mola, and G. Rozza. Dimension reduction in heterogeneous parametric spaces with application to naval engineering shape design problems. *Advanced Modeling and Simulation in Engineering Sciences*, 5(1):25, Sep 2018.
- [40] J. A. Tropp. User-Friendly Tail Bounds for Sums of Random Matrices. *Foundations of computational mathematics*, 12(4):389–434, 2012.
- [41] C. K. Williams and C. E. Rasmussen. *Gaussian Processes for Machine Learning*. Adaptive Computation and Machine Learning series. MIT press Cambridge, MA, 2006.
- [42] Q. Wu, F. Liang, and S. Mukherjee. Localized sliced inverse regression. *Journal of Computational and Graphical Statistics*, 19(4):843–860, 2010.
- [43] O. Zahm, P. G. Constantine, C. Prieur, and Y. M. Marzouk. Gradient-based dimension reduction of multivariate vector-valued functions. *SIAM Journal on Scientific Computing*, 42(1):A534–A558, 2020.
- [44] O. Zahm, T. Cui, K. Law, A. Spantini, and Y. Marzouk. Certified dimension reduction in nonlinear Bayesian inverse problems. *arXiv preprint arXiv:1807.03712*, 2018.
- [45] G. Zhang, J. Zhang, and J. Hinkle. Learning nonlinear level sets for dimensionality reduction in function approximation. In *Advances in Neural Information Processing Systems*, pages 13199–13208, 2019.